Research Square

Preprints are preliminary reports that have not undergone peer review.
They should not be considered conclusive, used to inform clinical practice,
or referenced by the media as validated information.

Biotic and Abiotic Sources of Stress on Wild Rocket Classified by Leaf-image Hyperspectral Data Mining With an Artificial Intelligence Model

Alejandra Navarro (alejandra.navarrogarcia@crea.gov.it)
Consiglio per la ricerca in agricoltura e l'analisi dell'economia agraria https://orcid.org/0000-0003-3406-7417

Nicola Nicastro
CREA Centro di Ricerca Orticoltura e Florovivaismo

Corrado Costa
CREA-IT: CREA Centro di Ricerca Ingegneria e Trasformazioni Agroalimentari

Alfonso Pentangelo
CREA Centro di Ricerca Orticoltura e Florovivaismo

Mariateresa Cardarelli
CREA Centro di Ricerca Orticoltura e Florovivaismo

Luciano Ortenzi
CREA-IT: CREA Centro di Ricerca Ingegneria e Trasformazioni Agroalimentari

Federico Pallottino
CREA-IT: CREA Centro di Ricerca Ingegneria e Trasformazioni Agroalimentari

Teodoro Cardi
CREA Centro di Ricerca Orticoltura e Florovivaismo

Catello Pane
CREA Centro di Ricerca Orticoltura e Florovivaismo

Research

Keywords: Hyperspectral imaging, Fusarium wilting, Machine learning, Rhizoctonia rotting, Water deficit, Salinity

Posted Date: September 15th, 2021

DOI: https://doi.org/10.21203/rs.3.rs-889533/v1

License: This work is licensed under a Creative Commons Attribution 4.0 International License.
Read Full License

Biotic and abiotic sources of stress on wild rocket classified by leaf-image hyperspectral data mining with an artificial intelligence model

Alejandra Navarro[1,*], Nicola Nicastro[1], Corrado Costa[2], Alfonso Pentangelo[1], Mariateresa Cardarelli[1], Luciano Ortenzi[2], Federico Pallottino[2], Teodoro Cardi[1], Catello Pane[1]

[1] Council for Agricultural Research and Economics (CREA), Research Centre for Vegetable and Ornamental Crops, Via Cavalleggeri 25, 84098 Pontecagnano Faiano, Italy

[2] Consiglio per la ricerca in agricoltura e l'analisi dell'economia agraria (CREA) - Centro di ricerca Ingegneria e Trasformazioni agroalimentari, Via della Pascolare 16, 00015 Monterotondo, Italy

[*] Corresponding author:
Dr. Alejandra Navarro
CREA, Research Centre for Vegetable and Ornamental Crops
Via dei Cavalleggeri 25, 84098 Pontecagnano Faiano (SA), Italy
Phone: +39-089-386212
Fax: +39-089-384170
alejandra.navarrogarcia@crea.gov.it

Abstract

Background: Wild rocket (*Diplotaxis tenuifolia*) is prone to soil-borne stresses under intensive cultivation systems devoted to ready-to-eat salad chain, increasing needs for external inputs. Early detection of the abiotic and biotic stresses by using digital reflectance-based probes may allow optimization and enhance performances of the mitigation strategies.

Methods: hyperspectral image analysis was applied to *D. tenuifolia* potted plants subjected, in a greenhouse experiment, to five treatments for one week: a control treatment watered to 100% water holding capacity, two biotic stresses: Fusarium wilting and Rhizoctonia rotting, and two abiotic stresses: water deficit and salinity. Leaf hyperspectral fingerprints were submitted to an artificial intelligence pipeline for training and validating image-based classification models able to work in the stress range. Spectral investigation was corroborated by pertaining physiological parameters.

Results: Water status was mainly affected by water deficit treatment, followed by fungal diseases, while salinity did not change water relations of wild rocket plants compared to control treatment. Biotic stresses triggered discoloration in plants just in a week after application of the treatments, as evidenced by the colour space coordinates and pigment contents values. Some vegetation indices, calculated on the bases of the reflectance data, targeted on plant vitality and chlorophyll content, healthiness, and carotenoid content, agreed with the patterns of variations observed for the physiological parameters. Artificial neural network helped selection of VIS (492-504, 540-568 and 712-720 nm) and NIR (855, 900-908 and 970 nm) bands, whose read reflectance contributed to discriminate stresses by imaging.

Conclusions: This study provided significative spectral information linked to the assessed stresses, allowing the identification of narrowed spectral regions and single wavelengths due to changes in photosynthetically active pigments and in water status revealing the etiological cause.

KEYWORDS: Hyperspectral imaging; Fusarium wilting; Machine learning; Rhizoctonia rotting; Water deficit; Salinity

Background

Plant diseases or abiotic stresses, such as water deficit or salinity, are key factors in the growth and yield of most vegetable crops [1-5]. The early detection and identification of both biotic and abiotic stresses would provide an opportunity for early intervention to control, prevent spread of infection or change irrigation management practices before the whole crop is damaged and vast yield losses occur [6]. Imaging sensors can identify the onset of adverse stresses before visible symptoms appear. Among imaging techniques, hyperspectral imaging is preferable for the identification and categorization of early stages of plant foliar diseases and abiotic stresses from laboratory to field scale, since uses high-fidelity plant reflectance information over a large range of the light spectrum, beyond that human vision, capturing more than the usual three bands of coloured light found in traditional digital imaging.

Hyperspectral imaging has already been used in vegetable crops for detecting biotic or abiotic stress, such as water salinity in lettuce [7], water stress in potato [8] and in tomato [9], Sclerotinia disease on oilseed rape [10], downy mildew in cucumber [11], most important diseases in tomato, bell pepper, potato and squash [12]. In order to determine the best combination of reflectance wavelengths sensitive for diagnosing water or saline stress as well as plant diseases, hyperspectral images can be studied and used on rocket leaves before visible damages create a high detriment value in the production of this vegetable primarily employed for the fresh consumption of a ready-to-eat product, due to its unique taste.

Wild or perennial rocket [*Diplotaxis tenuifolia* (L.) D.C.], is a leafy vegetable, commonly also known as arugula, roquette or rucola, belonging to the mustard family (Brassicaceae). It's traditionally grown in the Mediterranean region, widely consumed in Italy, but with increasing popularity as green salad (mixed or alone) in other parts of the World thanks to its excellent nutritional

properties and its antioxidant activity [13-17]. The major producer area of wild rocket in the European Union is the Southwest of Italy, with an annual cultivation area of about 4,800 hectares under protected cultivation with yields ranging between about 30-40 kg m^{-2} of fresh cut [18, 19]. Sustainability of the wild rocket productive processes must be increased in terms of reduction of synthetic fungicides applications for the effective soil-borne disease control, and to improve the water use efficiency. Moreover, water management, also regarding crop tolerance to salinity attributable to the concentration of salts in the highly fertigated soils or the use of low-quality irrigation water, is due. All these factors affect plant sap-flow efficiency, compromising plant vitality and then, yield.

Fusarium oxysporum f. sp. raphani Kendrick & Snyder is the causal agent of the wild rocket wilting [20], while *Rhizoctonia solani* Kühn [telomorph *Thanatephorus cucumeris* (Frank) Donk] is a parenchymatic pathogen causing rotting on roots, crown and collar [21]. Both telluric pathogens provoke dramatic epidemics under favourable environmental conditions (i.e., inoculum accumulation, high humidity, and continuous cropping of susceptible cultivars) like those that occur in sick and intensively exploited soils [22]. Most Brassicas species have been categorized as moderately salt tolerant, with, however, a significant interspecific and intraspecific variation [23]. Contradictory findings exist regarding the reaction of these species to salt stress at different plant developmental stages, while most authors indicate that these species maintain their degree of salt tolerance consistently throughout the plant ontogeny.

So, to limit reduction of yields and avoid unexpected loss of earnings in the presence of the stress factors, the time-effective application of plant protection as well as water management correction is desirable [24, 25] if only with the help of the digital sensing. Actually, the soil-borne diseases, the water deficit and exceeding water salinity, in different way in the long run, may produce at canopy level, similar symptoms related to sap-flow deficiency, which could be difficult to discriminate at a quick visive inspection, especially on large scale.

Precision farming principles require to connect as much information as possible derived from sensing systems to develop support tools for farmer's decisions on the base of high throughput non-destructive monitoring capability applicable on large cultivated surfaces [26-28].

The goal of this experiment was to early detect and identify, through the hyperspectral image analysis, the biotic (Fusarium wilt and Rhizoctonia rot) and abiotic (water and saline) stressors causing symptoms on wild rocket, to extend its application in the future to most of leafy vegetables. Direct measurements of water status, leaf colour and pigment contents were performed to ascertain the sensibility of wild rocket to such biotic and abiotic stress sources and to bear out the effectiveness of hyperspectral image technique.

Materials and Methods

Plant pathogens

The phytopathogens used in this study were *R. solani* (AG-4) and *F. oxysporum f. sp. raphani* isolated from symptomatic cabbage and wild rocket plants, respectively. Both fungal strains are maintained on potato dextrose agar (PDA, Oxoid) slants at 20 °C and each isolate was preliminarily tested for pathogenicity on wild rocket cv Tricia. Pathogen inoculum preparation followed procedures described by Pane et al. [29, 30] to obtain *R. solani* infected millet and *F. oxysporum* conidial suspension, respectively.

Plant material and experimental conditions

The *in planta* experiment was carried out in the glasshouse of the CREA-Research Centre of Vegetable and Ornamental Crops (Pontecagnano Faiano, Italy). Wild rocket (cv Tricia) seedlings were transplanted (five *per* each) in 20 cm plastic pots filled with autoclaved soil-peat. Pots were arranged on bench and supplied with a basal NPK mix nutritive solution at three-day intervals until to about a month of growth. Then, plants were subjected to five treatments during 1 week: plants watered to 100% water holding capacity (leaching 20% of the applied water) (Control, C); infection

120 by drenching 100 mL pot^{-1} of *F. oxysporum f. sp. raphani* strain conidial suspension (1.0×10^5 conidia
121 mL^{-1}) (Fusarium stress, F); infection by amending 10 g pot^{-1} of *R. solani* colonized millet
122 (Rhizoctonia stress, R); plants received 50% of water than the control (well-watered) plants (Water
123 stress, W); plants irrigated at holding capacity, with electrical conductivity (EC) of the irrigation
124 solution of 3.7 dS m^{-1}, after addition of NaCl (saline stress, S). This research was executed in a
125 randomized complete block design with ten replications, and each replicate represented a pot with 5
126 plants.
127
128 *Water status*
129 The plant water status of rocket accessions was determined by the leaf relative water content
130 (RWC_l; %), the plant water potential (Ψ_{pl}; MPa), the osmotic potential at full turgor (Ψ_{100s}; MPa), the
131 electrolyte leakage (EL; %) and the dry matter content (DM; %). The RWC_l was measured in excised
132 leaves harvested at midday (10:30 - 12:30 h solar time) using one leaf per plant of three plants per
133 pot, providing an average pot RWC_l, for five pots per treatment, according to the equation (Barrs &
134 Weatherley, 1962):
135 $$RWC_l = \frac{FW-DW}{TW-DW} \times 100 \quad (1)$$
136 where FW, DW, and TW are the fresh, dry, and turgid weights (g), respectively, of the whole
137 leaf.
138 Leaves were weighed immediately after collection to determine the fresh weight (FW). The cut
139 end of each leaf was placed in distilled water and kept in dim light at 4 °C for 24–48 h till the turgid
140 weight (TW) was reached and recorded. The dry weight (DW) was measured after air-drying the
141 leaves at 70 °C for 48 h.
142 The determination of the Ψ_{pl} was estimated according to the method described by Scholander
143 et al. [31], using a pressure chamber (Model 600 EXP Super Chamber, PMS Instrument Company,
144 Albany, OR, USA) in five plants per treatment. The rocket plant was pulled out from the soil and the

soil was carefully washed away from the roots, which were immediately submerged in a container of water and placed in the pressure chamber. The upper part of the plant was detopped with a razor blade, sealed in the chamber and pressurised. The pressure in the pressure chamber was raised using nitrogen gas at a rate of 0.02 MPa s^{-1} [32].

The Ψ_{100s} was measured in excised leaves harvested at midday (10:30 - 12:30 h solar time) using one leaf per plant in five plants per treatment. Leaves were placed by their petiole into flasks of distilled water and kept overnight in dim light at 4 °C to reach full saturation. After that, leaves were dried by filter paper to eliminate surface water, wrapped in aluminium foil and immediately frozen in liquid nitrogen (-170 °C) and stored at -30 °C. Before the measurements, samples were thawed and leaf sap was extracted for immediate determination of osmolality (mOsmol kg^{-1}) using a freezing point osmometer (Osmomat 3000, Gonotec GmbH, Berlin, DE). The Ψ_{100s} in MPa was obtained by multiplying the osmolality with –2.479 (conversion factor at 25 °C; 33, 34).

Electrolyte leakage (EL) was determined as described by Lutts et al. [35]. Briefly, 10 pieces of leaves (10 × 10 mm) collected from four plants *per* plot were placed in individual vials containing 10 mL of distilled water. Samples were incubated at room temperature (25 °C) on a shaker (100 rpm) for 24 h. The initial electrical conductivity (EC_1) of the bathing solution was measured using a conductivity meter (model Metrohm 6.0915.100, Metrohm Herisau, Switzerland). To measure total electrolytes released from leaf tissues, vials were then autoclaved at 120 °C for 20 min. The same samples were then autoclaved at 120 °C for 20 min and cooled at 25 °C to obtain the final electrical conductivity (EC_2). The EL was calculated as:

$$EL(\%) = \frac{EC1}{EC2} \times 100 \quad (2)$$

The dry matter content (DM) of the plant was expressed as weight percentage in 3 plants per pot and 5 pots per treatment and was calculated as dry weight (DW)/fresh weight (FW)×100. In order to determine the DW, fresh plant material was dried in a thermo-ventilated oven at 70 °C until it reached a constant mass.

Leaf color and pigments content

CIELAB (L*a*b*) leaf color coordinates were measured using a CR-210 Chroma Meter (Minolta Corp., Osaka, Japan) on leaf per plant of three plants per pot and ten pots per treatment. Measurements were done in duplicate on the two opposite lobes excluding the central rib and expressed as L*, a*, b* values. L* indicates lightness/darkness (0 = black, 100 = white), a* describes intensity in green−red (where a positive number indicates redness and a negative number indicates greenness), and b* describes the intensity in blue−yellow (where a positive number indicates yellowness and a negative number indicates blueness). Chroma (C) and hue angle (h) were estimated by the a* and b* values using the following equations:

$$C = [(a^*)^2 + (b^*)]^{1/2} \quad (3)$$

$$h = \tan^{-1} \frac{b^*}{a^*} \quad (4)$$

Chroma indicates colour saturation, while hue is a measure of the angle in the CIELAB colour chart (0° or 360° indicates red hue, while angles below 270°, 180°, and 90° indicate blue, green, and yellow hue, respectively).

SPAD index was measured at the midpoint of one leaf per plant of three plants per pot and 20 pots per treatment, using a Minolta SPAD-502 chlorophyll meter (Konica-Minolta, Japan).

Chlorophylls (µg g^{-1} fresh weight) were extracted by homogenization of fresh leaf tissues (0.5 g) in acetone (80%). The resulting extracts were centrifuged at 4800× g for 15 min and the absorbance of solutions was measured at 662 and 647 for chlorophyll *a* and *b*, respectively, by a UV-Vis spectrophotometer (model UV-1800, Shimadzu, Canby, US). Formula and extinction coefficients used for the determination of chlorophylls were described by Lichtenthaler and Wellburn [36]. The total chlorophyll content was calculated as the sum of chlorophyll *a* and *b*.

Hyperspectral Imaging

195 Hyperspectral images were immediately acquired, once rocket leaves were detached, using the
196 SPECIM IQ camera (SPECIM, Spectral Imaging Ltd., Oulu, FI), working in the range of 400–1000
197 nm. A total of 204 wavelengths were considered along this range, with a probe spectral resolution of
198 7 nm. The camera carries a complementary metal-oxide-semiconductor (CMOS) sensor with a spatial
199 sampling of 512 pixels and an image spatial resolution of 512 × 512 pixels [37]. Reflectance value
200 was calculated automatically by the camera software. Two 46 W halogen lamps pointing at each
201 corner of the object were used for stable lighting conditions of the scene. One image *per* replicate,
202 containing 5 leaves, one for each treatment, was acquired, obtaining 30 images for a total of 150
203 leaves.

204 Samples were scanned by acquiring the entire surface of the leaf creating a hypercube dataset.
205 Relative reflectance hyperspectral images were simultaneously computed by the camera software.
206 White reference and dark frame and raw data were acquired during the measurement.

207 The equation for the computation of the Reflectance by the SPECIM IQ Camera is:

208 $$\text{Reflectance} = \frac{\text{Raw\_data}^{t1} - \text{Dark}^{t1}}{\text{Raw\_data}^{t2} - \text{Dark}^{t2}} \text{ x } \frac{t2}{t1} \quad (5)$$

209 The extraction of the spectral signature from each leaf was performed using the plugin of
210 Quantum GIS software, called Point Sampling Tools that allowed a random sampling, from three
211 regions of interest (ROIs) designed on the upper leaf surface on both sides and at the apex, of 10
212 pixel-point each, for a total of 30 spectral signature *per* leaf. The resulting dataset including 4500
213 spectra was submitted to the successive elaboration in section *Artificial intelligence modelling*.
214 Vegetation indexes were calculated by computing the spectral data according to the formulas reported
215 in Table S1.

216

217 *Statistical analyses*

218 Differences among treatments for parameters of sections "water status" and "leaf color and
219 *pigments content"* were analysed by one-way ANOVA test (at $P \leq 0.05$ level) followed by a Duncan

pairwise comparison test using Statgraphics Plus 5.1 (StatPoint Technologies Inc., Warrenton, VA, US).

Artificial intelligence modelling

The hyperspectral images aforementioned, section *Hyperspectral Imaging,* were analysed by means of an artificial intelligence approach aiming at classifying the spectra associated with the single pixel of the image. For each leaf, mean spectral values of the 204 wavelengths were calculated, and the dataset submitted for the artificial intelligence modelling was composed by 150 observations (*i.e.* 30 leaves for each class) × 204 wavelengths. To do this, a single layer feed forward artificial neural network (SLFN; 38) was designed using a one-hidden layer architecture with 40 nodes and sigmoid activation functions and 5 SoftMax output neurons associated respectively with the following classes: control, Fusarium, Rhizoctonia, Salinity stress and water stress. The artificial neural network (ANN) was trained with Scaled conjugate gradient backpropagation algorithm [39] as implemented in the deep learning MATLAB toolbox. The dataset was partitioned using 70 percent of the samples (105) as training set and 30 per cent of the data set as test set (45). The test set was used to validate the model. This partitioning was optimally chosen with the Euclidean distances calculated by the algorithm reported by Kennard and Stone [40], selecting parameters without a priori knowledge of a regression model. The cost function was minimized using the mean squared normalized error (MSE) error performance function with a 10^{-10} threshold on the gradient.

The confusion matrix of the percentages of pixel classification for each leaf was produced and an ANOVA test (H_0: same mean) was performed to test the significance of differences between classified pixels into classes.

In order to understand which frequency values, among the 204 considered in the absorbance spectra, resulted to be more important in revealing the effects due to the presence of the different stresses, a variable impact analysis was also conducted. The variable impact Δ^k for the k-th frequency of the absorbance spectrum, was calculated in the following way. The complete data set (training set

+ test set) was considered made of *m* absorbance spectra. Each spectrum can be thought as a row vector **x** with *n* columns. The *m* spectra of the data set were stored in a matrix **X** having *m* rows and *n* columns. As a result, a generic element of that matrix is X_m^n. The spectra belong to 5 classes represented by a vector **y**. The output **y** is indeed a column vector with *m* rows obtained by applying the operator ***N*** to the matrix **X**:

$$\mathbf{y} = \boldsymbol{N}\mathbf{X} \tag{6}$$

In particular, $y = \boldsymbol{N}\mathbf{X_k}$ is a row number representing the class of the k-th element of the data set and X_k is the row vector representing the k-th row of the **X** matrix (*i.e.*, the k-th spectrum of the data set). In this study ***N*** is a nonlinear operator and can be expressed as the tensor product of several linear and nonlinear operators. It represents, indeed, the converged SLFN. As a first step the first row X_1 of the matrix **X** was considered and the operator ***N*** was applied *m* times to X_1, choosing each time a different value of X_1^1 among the values of X^1, the latter being the first column of the matrix **X**. The 1-case dependent variable impact of the first variable Δ_1^1 was then defined as:

$$\Delta_1^1 = \max_{X_1^1 \in X^1} \boldsymbol{N}X_1 - \min_{X_1^1 \in X^1} \boldsymbol{N}X_1 \tag{7}$$

This procedure was repeated for all the *n* variables over all the data set. The *i*-case dependent variable impact of the *k*-variable Δ_i^k was then defined as:

$$\Delta_i^k = \max_{X_i^k \in X^k} (\boldsymbol{N}X_i) - \min_{X_i^k \in X^k} (\boldsymbol{N}X_i) \tag{8}$$

Finally, the variable impact of the *k*-th frequency of the spectra was then obtained by averaging Δ_i^k over all the *m* cases of the data set:

$$\Delta^k = \frac{\sum_{i=1}^{m} \Delta_i^k}{m} \tag{9}$$

The procedure described above is similar to that implemented in the Palisade software. The model was developed by using the MATLAB 9.7 R2019b Deep Learning Toolbox.

Once the network has been trained, the artificial intelligence model was applied on each hyperspectral image, classifying pixel by pixel each entire image. The result of this operation was quantitative (i.e., counting the pixels belonging to each class).

Results

Water status of plants

Plant water status of wild rocket was determined at the end of the experimental period in the five treatments (Fig. 1). There were noticeable differences in water relations parameters, together with dry matter and SPAD index of wild rocket plants due to both abiotic and biotic stress sources applied (Table 1).

Table 1. Effects of the abiotic and biotic stresses sourced by *Fusarium oxysporum* f.sp. *raphani* (F), *Rhizoctonia solani* (R), salinity (S) and water deficit (W) compared to a healthy control (C), on the relative water content (RWC; %), plant water potential (Ψ_{pl}; MPa), osmotic potential at full turgor ($\Psi_{100\pi}$; MPa), electrolyte leakage (EL; %), dry matter (DM; %) and SPAD index (SPAD) in wild rocket seedlings at the end of the experimental period.

Treatments	**RWC (%)**		**Ψ_{pl} (MPa)**		**$\Psi_{100\pi}$ (MPa)**		**EL (%)**		**DM (%)**		**(SPAD)**	
C	89.29	a	-0.58	a[2]	-0.82	b	52.19	bc	9.95	b	50.85	a
F	83.60	b	-0.69	b	-0.68	a	83.22	a	11.15	ab	44.72	b
R	84.40	b			-0.93	c	79.07	a	13.81	a	45.01	b
S	78.51	b	-0.72	b	-0.84	b	47.88	c	10.63	b	50.48	a
W	71.92	c	-1.0	c	-0.84	b	72.08	ab	15.43	a	47.26	ab
P	***[1]		***		***		**		***		**	

[1] ** and *** denote statistical significance at the, 0.01 and 0.001 levels of significance, respectively.
[2] Different letters in the columns indicate significant differences between treatments, according to the Duncan's test ($P < 0.05$).

RWC and Ψ_{pl} behaved in a similar way, showing C plants the highest values of these parameters (90% and -0.58 MPa), while plants under water deficit showed the lowest RWC values (72%) and the most negative Ψ_{pl} (-1 MPa). For plants exposed to the other treatments (F, R, and S) intermediate values were found, although Ψ_{pl} was not measured in plants infected with *R. solani* due to its stem weakness. The lowest values of Ψ_{100s} were obtained in plants infected with *R. solani*, (-0.93 MPa) followed by abiotic stresses and C plants (on average -0.83 MPa), while highest values were found in plants infected with *F. oxysporum* f. sp. *raphani* (-0.68 MPa) (Table 1).

C and S treatment plants showed the lowest percentages of DM and EL (on average 50%) and the highest SPAD values (Table 1). The opposite happened for the biotic stressors and W treatments, which showed the highest EL percentages (on average 81% and 72% for biotic and W treatments, respectively) and the lowest SPAD values. The response of dry matter differed between biotic and W treatments, since plants under water stress showed the highest value of this parameter (15%), and in plants under biotic stressors this significant increase was only significative for plants infected with *R. solani* (≈ 14%) and not for those infected with *F. oxysporum* f. sp. *raphani* (11%) (Table 1).

In Figure 2 the colour coordinates, lightness, chroma, and hue angle which characterized leaf colour are showed. Lightness was increased with biotic stresses, although more pronounced in plants infected with *F. oxysporum* f. sp. *raphani,* compared C and abiotic stressors ones (Fig. 2a). For Chroma, the highest values were found in plants with F treatment and the lowest in S ones, the other treatments showing intermediate values (Fig. 2b). Hue angle decreased with biotic stresses in comparison with abiotic stresses and C treatments, and these values were statistically equal for the two fungal infections (Fig. 2c).

Chlorophyll *a* and carotenoids content showed a significant decrease only in plants infected with Fusarium compared to the other treatments, where values of these parameters were statistically equal (Fig. 3a, c). Reductions were on average of 50 and 20 μg g^{-1} for chlorophyll *a* and carotenoids, respectively. No differences among treatments were observed for chlorophyll *b* content (Fig. 3b).

VIS-NIR reflectance patterns and vegetation indices

Means of all pixel-wise spectral data from stressed and reference samples is showed in Figure 4, where an increased reflectance is highlighted around the photosynthetically active wavelengths in the VIS region for the Fusarium and Rhizoctonia samples compared to the other treatments. Forty-nine out of 54 hyperspectral vegetation indices considered in this study provided significant ($P \leq 0.05$) differences among treatments, in at least one case (Table S2). Twenty-four indices distributed along the various target categories of plant vitality and vegetation, pigment content and photochemical activity, were able to differentiate samples based on treatments. Interestingly, mSAVI, G, LIC3, RARS gNDVI and NDVI displayed a treatment rank ordering in agreement with physiological findings: Fusarium positioned at the opposite end of the control. WI was the lowest under Rizhoctotnia, whereas DVI, SAVI, TSAVI and REP were it for Fusarium. VARIg and mCARI were lower for S and W stresses, respectively, compared to the other treatments.

Artificial intelligence modelling based on VIS-NIR spectral data

The ANN trained model has a hidden layer size of 40 nodes and the algorithm converged after 955 iterations (3 seconds). Table 2 reports the characteristics and principal results of the ANN model used to predict the stress from the 150 (VIS-NIR) spectral data. All the 105 spectra in the training set were correctly classified. In testing, there were 12 misclassified spectra. The most misclassified stress was W (5 misclassified samples) followed by F (3 misclassified samples), R and S (2 misclassified samples). This was probably due to the spectral modification associated with the biological consequences induced by the 4 stresses (stoma enclosure and temperature enhancement). The trained ANN model was used as a pixel classifier on the multispectral images shown in Figure 5 where different colors refer to the different classes.

Table 2. Characteristics and principal results (number of cases, training time, number of trials, percentage of bad predictions) of the SLFN model (training and internal test) in predicting the classification of the different treatments: control, Fusarium, Rhizoctonia, salinity and water deficit.

Training (70%)	
Number of cases	105
Number of hidden layers	1
Number of nodes	40
Training time	00:00:03
Number of trials	955
% bad predictions	0.0
Testing (30%)	
Number of cases	45
% bad predictions (N)	26.7 (12)

The confusion matrix of the percentages of pixel classification for each leaf is reported in Table 3. The results of the ANOVA test (H_0: same mean) showed how percentages of correctly classified pixels (positioned on the main diagonal of the Table 3) are always significantly higher than those wrongly classified.

Table 3. Confusion matrix of the percentages of pixel classification for each leaf class, i.e. stresses sourced by *Fusarium oxysporum* f.sp. *raphani* (F), *Rhizoctonia solani* (R), salinity (S) and water deficit (W) compared to a healthy control (C). ANOVA test (H_0: same mean) results are reported using letters. Horizontally reading, equal letters correspond to no significant differences.

	Output				
Treatments	**C**	**F**	**R**	**S**	**W**
C	0.34 ± 0.10a	0.14 ± 0.07bc	0.12 ± 0.06c	0.19 ± 0.09b	0.21 ± 0.10b
F	0.05 ± 0.06c	0.56 ± 0.18a	0.16 ± 0.10b	0.06 ± 0.08c	0.18 ± 0.09b
R	0.08 ± 0.11c	0.22 ± 0.13b	0.45 ± 0.19a	0.08 ± 0.09c	0.18 ± 0.11b
SA	0.16 ± 0.11bc	0.15 ± 0.08c	0.14 ± 0.08c	0.34 ± 0.08a	0.20 ± 0.09b
WS	0.10 ± 0.07c	0.21 ± 0.14b	0.20 ± 0.13b	0.12 ± 0.09c	0.37 ± 0.12a

Observing the variable impact of spectral values, the most informative ones ranged within the following frequencies: 492-504 nm, 540-568 nm, 712-720 nm, 855 nm, 900-908 nm and 970 nm (Fig. 6).

Discussion

Wild rocket baby-leaf is currently cultivated under very intensive greenhouse farming essentially conditioned by relative humidity, fertigation, coastal soils and climate conditions, high seeding density, and the continuous re-cropping in monosuccession, which potentially expose crops to various biotic and/or abiotic stressors [41, 42]. The success of the managing strategies aimed at assuring the best growth settings of the plants in order to reach the expected yields and earns, relies on the early identification and on the targeted control of the etiological factors. Hyperspectral imaging has been proposed, in recent years, for the rapid, non-destructive and object-focused classification of plant physiological changes induced by the detrimental pathogen pressure and/or by plant growth adverse environmental conditions [43]. The digital checking of the plant stress onset may improve control methods efficacy by supporting farmer's decisions and quickly advising for and precise intervention.

The current study focused on wild rocket deficiencies possibly caused by two soil-borne pathogens, *F. oxysporum* f. sp. *raphani* and *R. solani*, and two abiotic stress-sources ascribed to water deficit and salinity. The related aboveground symptoms may be not properly distinguishable by visual tracking, and, especially in the early stages of their evolution, they can be confused among them, delaying the application of most appropriate remedies. Root system is the major target of salt and drought in the soil and can modulate physiological responses in the aerial part of plant, translating into non-specific symptoms as result of the affected nutrient flux and water relations [44].

In the current study, water relations of wild rocket plants, were mainly affected by abiotic stress, as shown by decreases in RWC and Ψ_{pl}, but with higher impact for water deficit, where higher EL and DM were also found. The rates of passive ion leakage (EL) from stress damage plant tissue are used as a measure of alterations in membrane permeability, and for characterizing cell membrane plants stability [45], suggesting that plant cell membranes were damaged under water deficit in this study. Instead, plants under salinity conditions showed the same values of EL and DM that control ones,

and values of RWC and Ψ_{pl} lower that in C plants but statistically higher than in W treatment, due on one hand to the short-term exposure to sodium chloride and on the other for the known tolerance of rockets plants to salinity. Barbieri et al. [46], established an EC of 5 dS m^{-1} in the nutrient solution for an improvement in dry matter content, visual appearance, carotenoids and phenols of *E. sativa*, while Bonasia et al. [47] give a threshold of the EC of 3.5 dS m^{-1} in the nutrient solution for growing wild rocket, which enhances leaf consistence, visual quality, and antioxidant compounds, and reduces the nitrate content, without dry weight decrease. Indeed, saline stress have been applied by other authors [48, 49] to improve the quality of vegetables, increasing the production of secondary metabolites and sensorial traits and reducing anti-nutritional factors.

At the beginning of the Rhizoctonia basal rotting and Fusarium wilting, wild rocket plants decreased their RWC and Ψ_{pl} (no data for Rhizoctonia disease) as well as it happened under abiotic stresses. However, the Ψ_{100s} highlights a variable response among biotic factors, likely in relation to the specificity of stressors mechanisms in damaging plant. The lowest values of Ψ_{100s} found in plants infected with *R. solani,* comparing to other treatments, are indicative of osmotic adjustment, which involves the net accumulation of solutes in a cell in response to a stress. Pérez-Pérez et al. [50] stated that, consequently, the osmotic potential decreases, which in turn attracts water into the cell and enables turgor to be maintained, although it was not possible to know the entity of plant stress since it was not able to measure Ψ_{pl} in plants infected with *R. solani*. *F. oxysporum f. sp. raphani* enters the host through the root and therefore develops endophytically until invades the xylem vessels, not externally as happens with *R. solani*. Plants under Fusarium infection use as defence reaction the production of physical barriers (i.e. gums) in order to block pathogen progression. Nevertheless, vessel occlusion prevents the mycelium spreading, but also dramatically reduces the entrance of solutes and water from root medium. As consequence their Ψ_{100s} did not decrease, nay values were even higher than in control plants, suggesting a decrease of turgor potential (Ψ_t). Ψ_{pl} reflect the symptoms of a water stress in the plant, but the relative contribution of the two main components (Ψ_s

409 and Ψ_t) to leaf water potential can experiment significant differences depending on the species and/or
410 treatment (stress) applied. Increased resistance of water flow from the substratum to the plant has
411 been observed in numerous species, especially under water stress conditions [51-53] and, in our case
412 this phenomenon could have reduced water transport towards the leaves due to the gradual closure of
413 xylem vessels due to Fusarium mycelium. Furthermore, both fungi strongly increased the electrolyte
414 leakage suggesting that stress-induced injury of cell membrane due to the oxidative damage, could
415 be related with the turgor loss.

416 Colour space coordinate values suggested that the leaves of plants under biotic stresses were a
417 yellower green (decreased hue angle), lighter (increased lightness) and gain in saturation (increased
418 chroma) compared with the leaves of C plants and those of abiotic stresses. This indicates that leaf
419 colour is modified by biotic stresses, and that, the discoloration resulting from both pathogens could
420 be due to chlorophyll breakdown as also suggested by the lowest SPAD values. However,
421 spectrophotometric assessments of pigments revealed significant reduction of the chlorophyll *a* and
422 *b*, and carotenoids content only in Fusarium diseased plants with regard of the compared treatments.
423 As it was demonstrated on tomato, xylem flux decline due to Fusarium wilting is very detrimental for
424 the photosynthetic system deprived of active pigments already at 6-8 days after infection started [54].
425 In contrast, *R. solani* did not affect chlorophyll concentration, as it was previously observed on
426 Chinese cabbage in a comparable time frame [55].

427 Some vegetation indices, calculated on the bases of the reflectance data, targeted on plant
428 vitality and chlorophyll content (NDVI and G), healthiness (mSAVI), and carotenoid content (LIC3
429 and RARS), proved to be in agreement with the patterns of variations observed for the physiological
430 parameters. Vegetation indices have been currently proposed as reliable method to classify plant
431 diseases and stresses by synthetizing hyperspectral outputs with the purpose of an early identification
432 [56]. They elaborate in narrower spectrum data ranges that carry biological meanings. In the current
433 study, for the first time, an artificial intelligence model based on the leaf hyperspectral reflectance
434 has been developed obtaining very good performances (only 26.7% of bad predictions). The dataset

435 was further mined with and promising insights to perform an accurate classification of symptom
436 source were obtained. The Artificial Neural Network modelling by pixel classifier managed to
437 separate wild rocket treatments based on the significant differences occurring in the leaf hyperspectral
438 signatures attributing higher discriminative weight to restricted wavelength intervals 492-504 nm,
439 540-568 nm and 712-720 nm, respectively falling in the blue, green and red VIS ranges and to 855
440 nm, 900-908 nm and 970 nm of the NIR spectrum. The ANN-filtered those reflectance regions, which
441 have been previously individuated to refer about plant stresses since they were related to leaf pigments
442 and cell structures changes. Narrowed blue and red ranges were previously found to be indicative of
443 shifts in leaf absorption by pigments [57] and in chlorophyll content [58] due to ongoing plant
444 stresses. Recently, a trained Random Forest model have been applied to scout non-redundant bands
445 falling into violet-blue light region able to classify powdery mildew-affected wild rocket leaves [59].
446 Reflectance wavebands within green pigment indices selected by optimal wavelet-based regression
447 model as predictor of active chlorophyll quantification [60]. Gitelson et al. [61] exploiting the high
448 sensitivity of the VIS green channel to chlorophyll *a* concentration tailored the green-NDVI index
449 with the purpose of monitoring photosynthetic activity and related-plant stresses. As matter of the
450 fact, in this study, gNDVI values proved to be gradated on the stress magnitude of treatments as well
451 as G index, calculated as R_{550}-to-R_{670} simple ratio, LIC3 (R_{440}/R_{730}) and RARS (R_{746}/R_{513}). Instead,
452 PRI, calculated on R_{531} and R_{570}, clearly separated stressed from non-stressed samples at the very
453 precocious stages of the current experimental conditions. Photochemical reflectance index has been
454 proposed by Meroni et al. [62] for the remote early detection of an incipient ozone stress on white
455 clover, while on barley, it has detected drought stress at 8 days after the complete water deprivation
456 [63].

457 On the other hand, reflectance in the 950–970 nm region was found indicative of plant water
458 status in gerbera, while, on the same crop, the R_{970}-to-R_{900} ratio closely tracked shifts in relative water
459 content [64]. As matter of fact, PRI and WI were found among the most sensitive hyperspectral

460 indices for the water status evaluation of tomato under different irrigation regimes [65] and of wheat
461 under genetic selection for drought resistance [66].

462 Similar findings were previously observed on sugar beet, where nematode-induced posterior
463 drought and Rhizoctonia wilting were significantly classified by canopy imaging with the
464 carotenoids/chlorophyll *a* dependent SIPI (structural independent pigment index), SRPI (simple ratio
465 pigment index), and WI (water index) indices [67]. Analogously, Susič et al. [68] used a partial least
466 square-support vector machine (PLS-SVM) approach to individuate wavebands in shortwave infrared
467 spectral regions high discriminatory of tomato canopy response to root-knot nematodes and soil water
468 deficiency. In this regard, the experimental pipeline able to classify stresses just after 12 days from
469 the beginning has been described by Žibrat et al. [69]. Applying a linear regression analysis,
470 Manganiello et al. [70] recently found interactive combination of hyperspectral vegetation indices
471 TSAVI + SAVI and TVI able to predict baby-leaf infection levels of three different soil-borne
472 pathogens, including *R. solani* on wild rocket, as modulated by treatments with *Trichoderma* spp.
473 biocontrol agents.

474 Findings of the present work constitute a precious hyperspectral data collection about the
475 identification of putative bands for the wild rocket multiple stresses monitoring, to employ, in
476 perspective, as input light-filter of cheaper and feasible devices for the precision stress assessment in
477 this species, and extendable to other leafy vegetables. This study provided significative spectral
478 information linked to the assessed stresses as corroborated by the physiological measurements. The
479 potential of the hyperspectral technology to obtain innovative and high-performing detection tools is
480 here valorised by artificial neural network-based model that allowed the identification of narrowed
481 spectral regions and single wavelengths very sensitive to precocious shifts in reflectance profiles of
482 stressed wild rocket due to changes in photosynthetically active pigments (VIS: 492-504, 540-568
483 and 712-720 nm) and in water status (NIR: 855, 900-908 and 970 nm). The information is spendable
484 in the field of the technological innovation regarding to the conception of new optoelectronic probes
485 to serve farmers in supporting their choices.

Availability of data and materials

The datasets and field sampling data used in this study are available from the corresponding author on reasonable request.

References

1. González-Chavira MM, Herrera-Hernández MG, Guzmán-Maldonado H, Pons-Hernández JL. Controlled water deficit as abiotic stress factor for enhancing the phytochemical content and adding-value of crops. Sci Hortic. 2018; 234:354–360. https://doi.org/10.1016/j.scienta.2018.02.049.
2. Mariani L, Ferrante A. Agronomic management for enhancing plant tolerance to abiotic stresses-drought, salinity, hypoxia, and lodging. Horticulturae. 2017; 3(4):52. https://doi.org/10.3390/horticulturae3040052.
3. Savary S, Ficke A, Aubertot JN, Hollier C. Crop losses due to diseases and their implications for global food production losses and food security. Food Sec. 2012; 4:519–537. https://doi.org/10.1007/s12571-012-0200-5.
4. Oerke E.C. Crop losses to pests. J Agric Sci. 2006; 144:31–43. https://doi.org/10.1017/S0021859605005708.
5. Lamsal K, Paudyal GN, Saeed M. Model for assessing impact of salinity on soil water availability and crop yield. Agric Water Manag. 1999; 41:57–70. https://doi.org/10.1016/S0378-3774(98)00116-4.
6. Lowe A, Harrison N, French AP. Hyperspectral image analysis techniques for the detection and classification of the early onset of plant disease and stress. Plant Methods. 2007; 13:80. https://doi.org/10.1186/s13007-017-0233-z.

7. Lara MA, Diezma B, Lleó L, Roger JM, Garrido Y, Gil MI, Ruiz-Altisent M. Hyperspectral imaging to evaluate the effect of irrigation water salinity in lettuce. Appl Sci. 2016; 6:412. https://doi.org/10.3390/app6120412.
8. Amatya S, Karkee M, Alva A.K, Larbi P, Adhikari B. Hyperspectral imaging for detecting water stress in potatoes. ASABE. 2012; DOI:10.13031/2013.42218.
9. Elvanidi A, Katsoulas N, Ferentinos KP, Bartzanas T, Kittas C. Hyperspectral machine vision as a tool for water stress severity assessment in soilless tomato crop. Biosyst Eng. 2018; 165:25-35. https://doi.org/10.1016/j.biosystemseng.2017.11.002.
10. Kong W, Zhang C, Huang W, Liu F, He Y. Application of hyperspectral imaging to detect *Sclerotinia sclerotiorum* on oilseed rape stems. Sensors. 2018; 18(1):123. https://doi.org/10.3390/s18010123.
11. Tian Y, Zhang L. Study on the methods of detecting cucumber downy mildew using hyperspectral imaging technology. Phys Procedia. 2012; 33:743–750. https://doi.org/10.1016/j.phpro.2012.05.130.
12. Mohanty SP, Hughes D, Salathe M. Using deep learning for image-based plant disease detection. Front Plant Sci. 2016; 7:1419. https://doi.org/10.3389/fpls.2016.01419.
13. Hall MKD, Jobling JJ, Rogers GS. Some perspectives on rocket as a vegetable crop: a review. Veg Crop Res Bull. 2012; 76:21–41. DOI: 10.2478/v10032-012-0002-5.
14. Villatoro-Pulido M, Priego-Capote F, Álvarez-Sánchez B, Saha S, Philo M, Obregón-Cano S, De Haro-Bailón A, Font R, Del Río-Celestino M. An approach to the phytochemical profiling of rocket [*Eruca sativa* (Mill.) Thell]. J Sci Food Agric. 2013; 93:3809–3819. https://doi.org/10.1002/jsfa.6286.
15. Cavaiuolo M, Ferrante A. Nitrates and glucosinolates as strong determinants of the nutritional quality in rocket leafy salads. Nutrients. 2014; 6:1519-1538. https://doi.org/10.3390/nu6041519.

16. Alqasoumi S, Al-Sohaibani M, Al-Howiriny T, Al-Yahya M, Rafatullah S. Rocket '*Eruca sativa*': A salad herb with potential gastric anti-ulcer activity. World J Gastroenterol. 2009;15: 1958–1965. DOI:10.3748/wjg.15.1958.

17. Katsarou D, Omirou M, Liadaki K, Tsikou D, Delis C, Garagounis C, Krokida A, Zambounis A, Papadopoulou KK. Glucosinolate biosynthesis in *Eruca sativa*. Plant Physiol Biochem. 2016; 109:452–466. https://doi.org/10.1016/j.plaphy.2016.10.024.

18. Caruso G, De Pascale S, Nicoletti R, Cozzolino E, Rouphael Y. Productivity, nutritional and functional qualities of perennial wall-rocket: Effects of pre-harvest factors. Folia Hort. 2019; 31:71-80. DOI:10.2478/fhort-2019-0004.

19. Candido V, Boari F, Cantore V, Castronuovo D, Di Venere D, Perniola M, Sergio L, Viggiani R, Schiattone MI. Interactive effect of nitrogen and azoxystrobin on yield, quality, nitrogen and water use efficiency of wild rocket in southern Italy. Agronomy. 2020; 10:849. https://doi.org/10.3390/agronomy10060849.

20. Garibaldi A, Gilardi G, Gullino ML. Evidence for an expanded host range of *Fusarium oxysporum f. sp. raphani*. Phytoparasitica. 2006; 34:115–121. https://doi.org/10.1007/BF02981311.

21. Gilardi G, Gullino ML, Garibaldi A. New diseases of wild and cultivated rocket in Italy. Acta Hortic. 2013; 1005:569-572. DOI: 10.17660/ActaHortic.2013.1005.70.

22. Caruso G, Parrella G, Giorgini M, Nicoletti R. Crop systems, quality and protection of *Diplotaxis tenuifolia*. Agriculture. 2018; 8:55. https://doi.org/10.3390/agriculture8040055.

23. Ashraf M, McNeilly T. Salinity tolerance in Brassica oilseeds. Crit Rev Plant Sci. 2004; 23:157–174. https://doi.org/10.1080/07352680490433286.

24. Nicoletti R, Raimo F, Miccio G. *Diplotaxis tenuifolia*: biology, production and properties. Eur J Plant Sci Biotech. 2007; 1:36–43.

25. Caruso G, Stoleru V, De Pascale S, Cozzolino E, Pannico A, Giordano M, Teliban G, Cuciniello A, Rouphael Y. Production, leaf quality and antioxidants of perennial wall rocket

561 as affected by crop cycle and mulching type. Agronomy. 2019; 9:194.
562 https://doi.org/10.3390/agronomy9040194.
563 26. Caballero D, Calvini R, Amigo JM. 2020. Hyperspectral imaging in crop fields: precision
564 agriculture. In: Amigo JM, Editors. Data Handling in Science and Technology. Elsevier; 2020.
565 32:453-473. https://doi.org/10.1016/B978-0-444-63977-6.00018-3.
566 27. Feng X, Zhan Y, Wang Q, Yang X, Yu C, Wang H, Tang ZY, Jiang D, Peng C, He Y.
567 Hyperspectral imaging combined with machine learning as a tool to obtain high-throughput
568 plant salt-stress phenotyping. Plant J. 2020; 101:1448-1461.
569 https://doi.org/10.1111/tpj.14597.
570 28. Barreto A, Paulus S, Varrelmann M, Mahlein AK. Hyperspectral imaging of symptoms
571 induced by *Rhizoctonia solani* in sugar beet: comparison of input data and different machine
572 learning algorithms. J Plant Dis Prot. 2020; 127:441-451. https://doi.org/10.1007/s41348-
573 020-00344-8.
574 29. Pane C, Piccolo A, Spaccini R, Celano RG, Villecco D, Zaccardelli M. Agricultural waste-
575 based composts exhibiting suppressivity to diseases caused by the phytopathogenic soil-borne
576 fungi *Rhizoctonia solani* and *Sclerotinia minor*. Appl Soil Ecol. 2013; 65:43-51.
577 https://doi.org/10.1016/j.apsoil.2013.01.002.
578 30. Pane C, Sigillo L, Caputo M, Serratore G, Zaccardelli M, Tripodi P. Response of rocket salad
579 germplasm (*Eruca* and *Diplotaxis spp.*) to major pathogens causing damping-off, wilting and
580 leaf spot diseases. Arch Phytopathol Pflanzenschutz. 2017; 50(3-4):167-177, DOI:
581 10.1080/03235408.2017.1285511.
582 31. Scholander PF, Hammel HT, Bradstreet ED, Hemingsen EA. Sap pressure in vascular plants.
583 Science. 1965; 148:339-346. DOI: 10.1126/science.148.3668.339.
584 32. Turner NC. Measurement of plant water status by the pressure chamber technique. Irrig Sci.
585 1988; 9:289-308. https://doi.org/10.1007/BF00296704.
586 33. Taiz L, Zeiger E. Plant Physiology. 4th Edition, Sinauer Associates Inc., Sunderland, 2006

587 34. Pariyar S, Eichert T, Goldbach HE, Hunsche M, Burkhardt J. The exclusion of ambient
588 aerosols changes the water relations of sunflower (*Helianthus annuus*) and bean (*Vicia faba*)
589 plants. Environ Exp Bot. 2013; 88:43–52. https://doi.org/10.1016/j.envexpbot.2011.12.031.
590 35. Lutts S, Kinet JM, Bouharmont J. Changes in plant response to NaCl during development of
591 rice (*Oryza sativa* L.) varieties differing in salinity resistance. J Exp Bot. 1995; 46:1843–
592 1852. https://doi.org/10.1093/jxb/46.12.1843.
593 36. Lichtenthaler H, Wellburn A. Determinations of total carotenoids and chlorophylls a and b of
594 leaf extracts in different solvents. Biochem Soc Trans. 1983; 603:591-592.
595 https://doi.org/10.1042/bst0110591.
596 37. Behmann J, Acebron K, Emin D, Bennertz S, Matsubara S, Thomas S, Bohnenkamp D, Kuska
597 MT, Jussila J, Salo H, Mahlein AK, Rascher U. Specim IQ: Evaluation of a New, Miniaturized
598 Handheld Hyperspectral Camera and Its Application for Plant Phenotyping and Disease
599 Detection. Sensors. 2018; 18:441. https://doi.org/10.3390/s18020441.
600 38. Hornik K, Stinchcombe M, White H. Multilayer Feedforward Networks are universal
601 approximators. Neural netw. 1989; 2(5):359-366. https://doi.org/10.1016/0893-
602 6080(89)90020-8.
603 39. Møller M. A scaled conjugate gradient algorithm for fast supervised learning. Neural Netw.
604 1993; 6(4):525-533. https://doi.org/10.1016/S0893-6080(05)80056-5.
605 40. Kennard RW, Stone LA. Computer Aided Design of Experiments. Technometrics. 1969;
606 11(1):137-148. DOI:10.1080/00401706.1969.10490666.
607 41. Marin A, Ferreres F, Barberá GG, Gil MI. Weather Variability Influences Color and Phenolic
608 Content of Pigmented Baby Leaf Lettuces throughout the Season. J Agric Food Chem. 2015;
609 63:1673-1681. https://doi.org/10.1021/acs.jafc.5b00120.
610 42. Gullino ML, Gilardi G, Garibaldi A. Ready-to-Eat Salad Crops: A Plant Pathogen's Heaven.
611 Plant Dis. 2019; 103:9. https://doi.org/10.1094/PDIS-03-19-0472-FE.

612 43. Lowe A, Harrison N, French AP. Hyperspectral image analysis techniques for the detection
613 and classification of the early onset of plant disease and stress. Plant Methods. 2017; 13:80.
614 https://doi.org/10.1186/s13007-017-0233-z.
615 44. Forni C, Duca D, Glick BR. Mechanisms of plant response to salt and drought stress and their
616 alteration by Rhizobacteria. Plant Soil. 2017; 410:335–356. DOI: 10.1007/s11104-016-3007-
617 x.
618 45. Kocheva KV, Kartseva T, Landjeva S, Georgiev G. Physiological response of wheat seedlings
619 to mild and severe osmotic stress. Cereal Res. Com. 2009; 37:199-208.
620 https://doi.org/10.1556/crc.37.2009.2.6.
621 46. Barbieri G, Bottino A, Di Stasio E, Vallone S, Maggio A. Proline and light as quality
622 enhancers of rocket (*Eruca sativa* Miller) grown under saline conditions. Scientia Hortic.
623 2011; 128:393–400. https://doi.org/10.1016/j.scienta.2011.02.010.
624 47. Bonasia A, Lazzizera C, Elia A., Conversa G. Nutritional, biophysical and physiological
625 characteristics of wild rocket genotypes as affected by soilless cultivation system, salinity
626 level of nutrient solution and growing period. Front Plant Sci. 2017; 8:300.
627 https://doi.org/10.3389/fpls.2017.00300.
628 48. Gruda N.. Do soilless culture systems have an influence on product quality of vegetables?. J
629 Appl Bot Food Qual. 2009; 82:141–147. DOI 10.18452/9433.
630 49. Hamilton JM, Fonseca JM. Effect of saline irrigation water on antioxidants in three
631 hydroponically grown leafy vegetables: *Diplotaxis tenuifolia*, *Eruca sativa*, and *Lepidium*
632 *sativum*. HortScience. 2010; 45:546–552. https://doi.org/10.21273/HORTSCI.45.4.546.
633 50. Pérez-Pérez JG, Robles JM, Tovar JC, Botía P. Response to drought and salt stress of lemon
634 "Fino 49" under field conditions: Water relations, osmotic adjustment and gas exchange. Sci
635 Hortic. 2009; 122:83–90. https://doi.org/10.1016/j.scienta.2009.04.009.
636 51. Sánchez-Blanco MJ, Rodríguez P, Morales MA, Ortuño MF, Torrecillas A. Comparative
637 growth and water relations of *Cistus albidus* and *Cistus monspeliensis* plants during water

638 deficit conditions and recovery. Plant Sci. 2002; 162:107–113. https://doi.org/10.1016/S0168-
639 9452(01)00540-4.
640 52. Navarro A, Álvarez S, Castillo M, Bañón S, Sánchez-Blanco MJ. Changes in tissue-water
641 relations, photosynthetic activity, and growth of *Myrtus communis* plants in response to
642 different conditions of water availability. J hortic sci biotechnol. 2009; 84(5):541-547.
643 https://doi.org/10.1080/14620316.2009.11512563.
644 53. De Herralde F, Biel C, Savé R, Morales MA, Torrecillas A, Alarcón JJ, Sánchez-Blanco MJ.
645 Effect of water and salt stresses on the growth, gas exchange and water relations in
646 *Argyranthemum coronopifoliun* plants. Plant Sci. 1998; 139:9–17.
647 https://doi.org/10.1016/S0168-9452(98)00174-5.
648 54. Pshibytko NL, Zenevich LA, Kabashnikova LF. Changes in the photosynthetic apparatus
649 during Fusarium wilt of tomato. Russ J Plant Physiol. 2006; 53:25-31.
650 https://doi.org/10.1134/S1021443706010031.
651 55. Kang SM, Radhakrishnan R, Lee IJ. *Bacillus amyloliquefaciens* subsp. plantarum GR53, a
652 potent biocontrol agent resist Rhizoctonia disease on Chinese cabbage through hormonal and
653 antioxidants regulation. World J Microbiol Biotechnol. 2015; 31:1517-1527.
654 https://doi.org/10.1007/s11274-015-1896-0.
655 56. Xue J, Su B. Significant remote sensing vegetation indices: a review of developments and
656 applications. J Sensors. 2017; Article ID 1353691. https://doi.org/10.1155/2017/1353691.
657 57. Carter GA. Responses of leaf spectral reflectance to plant stress. Am J Bot. 1993; 80:239-243.
658 https://doi.org/10.1002/j.1537-2197.1993.tb13796.x.
659 58. Gitelson AA, Gritz Y, Merzlyak MN. Relationships between leaf chlorophyll content and
660 spectral reflectance and algorithms for non-destructive chlorophyll assessment in higher plant
661 leaves. J Plant Physiol. 2003; 160:271-282. https://doi.org/10.1078/0176-1617-00887.
662 59. Pane C, Manganiello G, Nicastro N, Cardi T, Carotenuto F. Powdery Mildew Caused by
663 *Erysiphe cruciferarum* on Wild Rocket (*Diplotaxis tenuifolia*): Hyperspectral Imaging and

664 Machine Learning Modeling for Non-Destructive Disease Detection. Agriculture. 2021;
665 11(4):337. https://doi.org/10.3390/agriculture11040337.
666 60. Blackburn GA, Ferwerda JG. Retrieval of chlorophyll concentration from leaf reflectance
667 spectra using wavelet analysis. Remote Sens Environ. 2008; 112:1614-1632.
668 https://doi.org/10.1016/j.rse.2007.08.005.
669 61. Gitelson AA, Kaufman YJ, Merzlyak MN. Use of a green channel in remote sensing of global
670 vegetation from EOS-MODIS. Remote Sens Environ. 1996; 58:289-298.
671 https://doi.org/10.1016/S0034-4257(96)00072-7.
672 62. Meroni M, Rossini M, Picchi V, Panigada C, Cogliati S, Nali C, Colombo R. Assessing
673 steady-state fluorescence and PRI from hyperspectral proximal sensing as early indicators of
674 plant stress: the case of ozone exposure. Sensors. 2008; 8(3):1740-1754.
675 https://doi.org/10.3390/s8031740.
676 63. Römer C, Wahabzada M, Ballvora A, Rossini M, Panigada C, Behmann J, On JL, Thurau C,
677 Bauckhage C, Kersting K, Rascher U, Mer LP. Early drought stress detection in cereals:
678 simplex volume maximization for hyperspectral image analysis. Funct Plant Biol. 2012;
679 39:878-890. https://doi.org/10.1071/FP12060.
680 64. Peñuelas J, Filella I, Biel C, Serrano L, Savé R. The reflectance at the 950–970 nm region as
681 an indicator of plant water status. Int J Remote Sens. 1993; 14:1887-1905.
682 https://doi.org/10.1080/01431169308954010.
683 65. Ihuoma SO, Madramootoo CA. Sensitivity of spectral vegetation indices for monitoring water
684 stress in tomato plants. Comput Electron Agric. 2019; 163:104860.
685 https://doi.org/10.1016/j.compag.2019.104860.
686 66. El-Hendawy S, Al-Suhaibani N, Al-Ashkar I, Alotaibi M, Tahir MU, Solieman T, Hassan
687 WM. Combining Genetic Analysis and Multivariate Modeling to Evaluate Spectral
688 Reflectance Indices as Indirect Selection Tools in Wheat Breeding under Water Deficit Stress
689 Conditions. Remote Sens. 2020; 12(9):1480. https://doi.org/10.3390/rs12091480.

67. Hillnhütter C, Mahlein AK., Sikora RA, Oerke EC. Remote sensing to detect plant stress induced *Heterodera schachtii* and *Rhizoctonia solani* in sugar beet fields. Field Crops Res. 2011; 122:70-77. https://doi.org/10.1016/j.fcr.2011.02.007.

68. Susič N, Žibrat U, Širca S, Strajnar P, Razinger J, Knapič M, Vončina A, Urek G, Gerič Stare B. Discrimination between abiotic and biotic drought stress in tomatoes using hyperspectral imaging. Sens Actuators B Chem. 2018; 273:842-852. https://doi.org/10.1016/j.snb.2018.06.121.

69. Žibrat U, Susič N, Knapič M, Širca S, Strajnar P, Razinger J, Vončina A, Urek G, Gerič Stare B. Pipeline for imaging, extraction, pre-processing, and processing of time-series hyperspectral data for discriminating drought stress origin in tomatoes. MethodsX. 2019; 6:399-408. https://doi.org/10.1016/j.mex.2019.02.022.

70. Manganiello G, Nicastro N, Caputo M, Zaccardelli M, Cardi T, Pane C. Functional hyperspectral imaging by high-related vegetation indices to track the wide- spectrum Trichoderma biocontrol activity against soil-borne diseases of baby-leaf vegetables. Front Plant Sci. 2021. DOI: 10.338

Acknowledgements

Not applicable.

Funding

This work was financed by the Italian Ministry of Agriculture, Food and Forestry Policies (MiPAAF), through the AgriDigit programme - sub-project 'Tecnologie digitali integrate per il rafforzamento sostenibile di produzioni e trasformazioni agroalimentari (AgroFiliere)' (DM 36503.7305.2018 of 20/12/2018).

Author information

Affiliations

1. **Council for Agricultural Research and Economics (CREA), Research Centre for Vegetable and Ornamental Crops, Via Cavalleggeri 25, 84098 Pontecagnano Faiano, Italy.**

   Alejandra Navarro, Nicola Nicastro, Alfonso Pentangelo, Mariateresa Cardarelli, Teodoro Cardi & Catello Pane

2. **Consiglio per la ricerca in agricoltura e l'analisi dell'economia agraria (CREA) - Centro di ricerca Ingegneria e Trasformazioni agroalimentari, Via della Pascolare 16, 00015 Monterotondo, Italy.**

   Corrado Costa, Luciano Ortenzi & Federico Pallottino

Contributions

AN, AP and CP designed the experiments. AP, CP, AN, MC, LO, FP performed the experiments and determination. AN, NC, CP, CC, LO, and FP analyzed and elaborated the data. AN, CC and CP wrote the paper. CP and TC contributed to the writing-reviewing and editing, supervision, project administration, funding acquisition.

All authors read and approved the final manuscript.

Corresponding author

Correspondence to Alejandra Navarro.

Ethics declarations

Ethics approval and consent to participate

Not applicable.

Consent for publication

All authors agree to publish the final manuscript.

742 *Competing interests*

743 The authors declare that they have no known competing financial interests or personal
744 relationships that could have appeared to influence the work reported in this paper.

745

746 **Figure legends**

747

748 **Fig. 1**. Wild rocket at the end of exposure to stresses sources, *Fusarium oxysporum* f.sp. *raphani* (F),
749 *Rhizoctonia solani* (R), salinity (S) and water deficit (W) compared to a healthy control (C).

750

751 **Fig. 2**. Effects of the abiotic and biotic stress on the and colour parameters (L, CHROMA and HUE)
752 in wild rocket seedlings at the end of the exposure period to stresses sourced by *Fusarium oxysporum*
753 f.sp. *raphani* (F), *Rhizoctonia solani* (R), salinity (S) and water deficit (W) compared to a healthy
754 control (C). Each histogram represents the mean of 6 values, and vertical bars indicate standard errors.
755 Different letters in histograms indicate significant differences between treatments, according to the
756 Duncan's test ($P<0.05$). ** and *** denote statistical significance at the 0.01 and 0.001 levels of
757 significance, respectively.

758

759 **Fig. 3.** Effects of the abiotic and biotic stress on chlorophyll and carotenoids content (Chl a, Chl b
760 and carotenoids; $\mu g\ g^{-1}$ DW) in wild rocket at the end of the exposure period to stresses sourced by
761 *Fusarium oxysporum* f.sp. *raphani* (F), *Rhizoctonia solani* (R), salinity (S) and water deficit (W)
762 compared to a healthy control (C). Each histogram represents the mean of 6 values, and vertical bars
763 indicate standard errors. Different letters in histograms indicate significant differences between
764 treatments, according to the Duncan's test ($P<0.05$). ns and *** denote not significant and statistical
765 significance at 0.001 level of significance, respectively.

766

Fig. 4. Hyperspectral reflectance signature in VIS-NIR spectral region of leaves from wild rocket exposed to various stresses sourced by *Fusarium oxysporum* f.sp. *raphani* (F, green), *Rhizoctonia solani* (R, blue), salinity (S, yellow) and water deficit (W, pink) compared with healthy control (C, red).

Fig. 5. Example of single pixel classification. Original image (in RGB; A) and classified image (B) through the trained ANN model used as a pixel classifier on the multispectral images. In B the colors refer to the different classes, i.e. wild rocket exposed to stresses sourced by *Fusarium oxysporum* f.sp. *raphani* (F, green), *Rhizoctonia solani* (R, blue), salinity (S, yellow) and water deficit (W, pink) compared with healthy control (C, red).

Fig. 6. Mean VIS-NIR spectral data (left side axis). Variable impact (right side axis) evidenced with blue line.

Figures

Figure 1

Wild rocket at the end of exposure to stresses sources, Fusarium oxysporum f.sp. raphani (F), Rhizoctonia solani (R), salinity (S) and water deficit (W) compared to a healthy control (C).

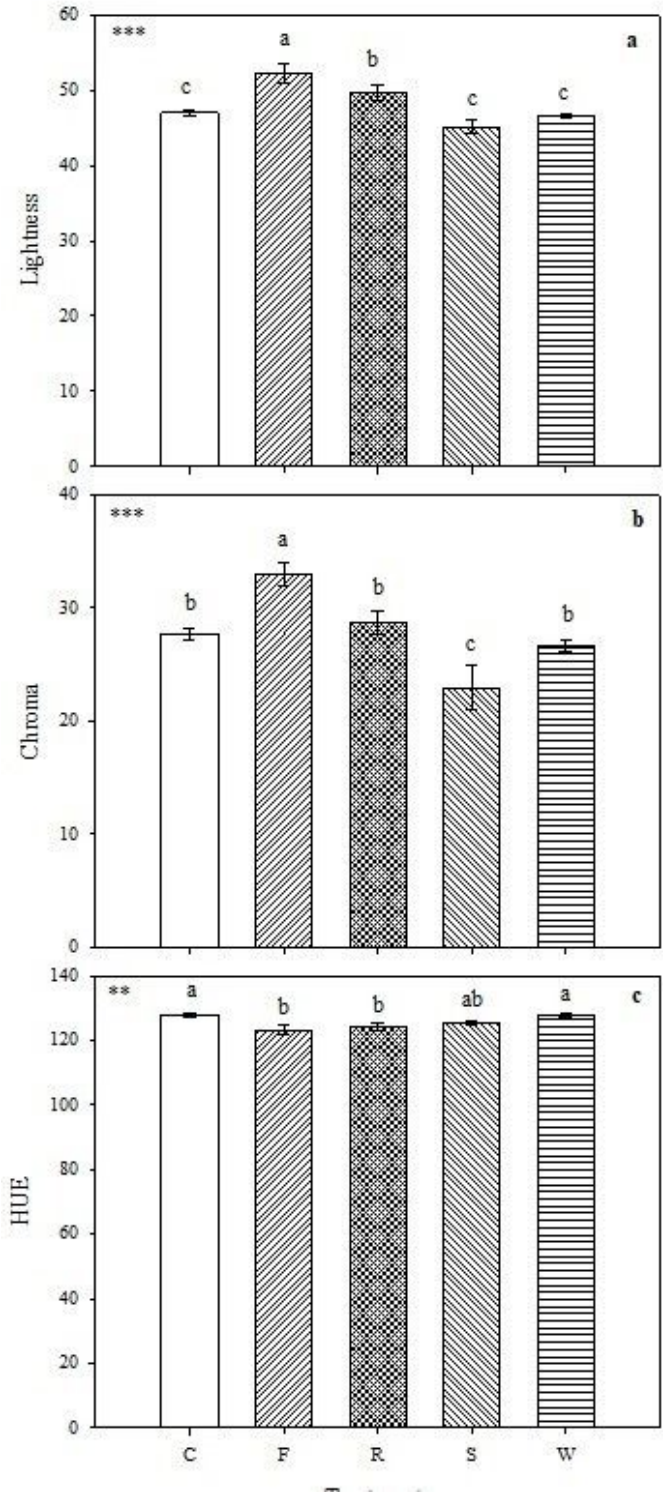

Figure 2

Effects of the abiotic and biotic stress on the and colour parameters (L, CHROMA and HUE) in wild rocket seedlings at the end of the exposure period to stresses sourced by Fusarium oxysporum f.sp. raphani (F), Rhizoctonia solani (R), salinity (S) and water deficit (W) compared to a healthy control (C). Each histogram represents the mean of 6 values, and vertical bars indicate standard errors. Different letters in

histograms indicate significant differences between treatments, according to the Duncan's test (P<0.05). ** and *** denote statistical significance at the 0.01 and 0.001 levels of significance, respectively.

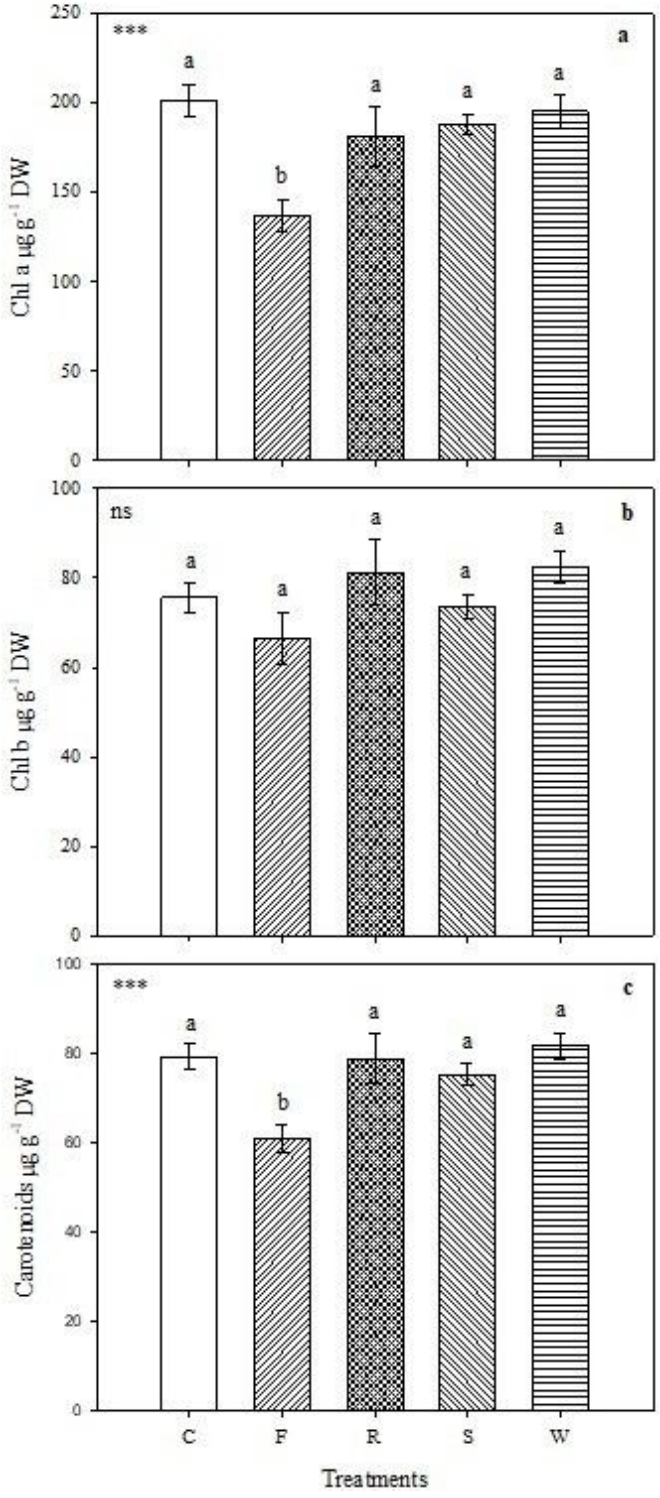

Figure 3

Effects of the abiotic and biotic stress on chlorophyll and carotenoids content (Chl a, Chl b and carotenoids; □g g-1 DW) in wild rocket at the end of the exposure period to stresses sourced by Fusarium oxysporum f.sp. raphani (F), Rhizoctonia solani (R), salinity (S) and water deficit (W) compared to a

healthy control (C). Each histogram represents the mean of 6 values, and vertical bars indicate standard errors. Different letters in histograms indicate significant differences between treatments, according to the Duncan's test (P<0.05). ns and *** denote not significant and statistical significance at 0.001 level of significance, respectively.

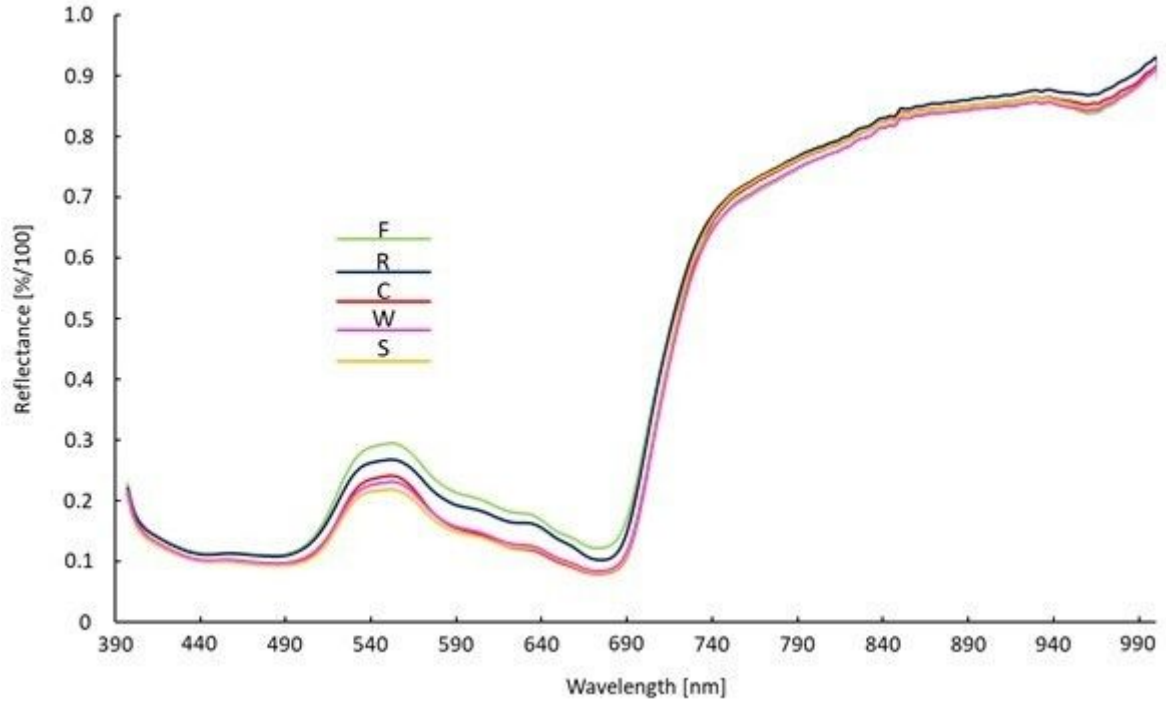

Figure 4

Hyperspectral reflectance signature in VIS-NIR spectral region of leaves from wild rocket exposed to various stresses sourced by Fusarium oxysporum f.sp. raphani (F, green), Rhizoctonia solani (R, blue), salinity (S, yellow) and water deficit (W, pink) compared with healthy control (C, red).

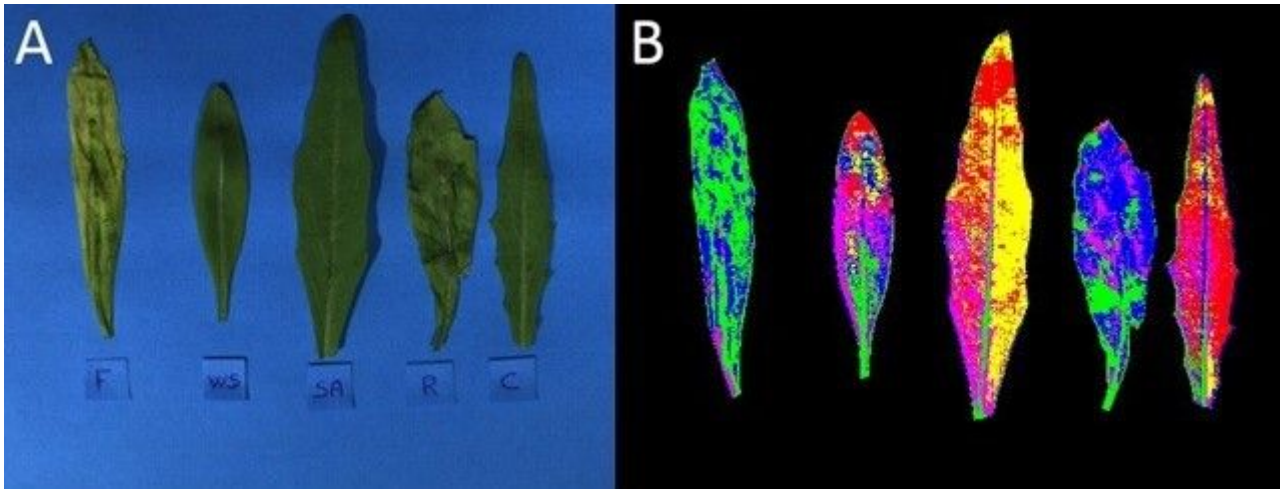

Figure 5

Example of single pixel classification. Original image (in RGB; A) and classified image (B) through the trained ANN model used as a pixel classifier on the multispectral images. In B the colors refer to the

different classes, i.e. wild rocket exposed to stresses sourced by Fusarium oxysporum f.sp. raphani (F, green), Rhizoctonia solani (R, blue), salinity (S, yellow) and water deficit (W, pink) compared with healthy control (C, red).

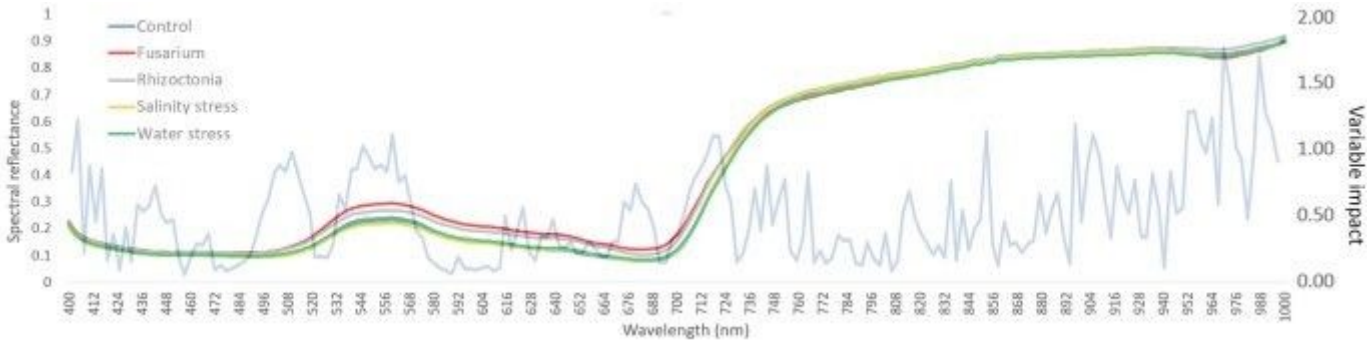

Figure 6

Mean VIS-NIR spectral data (left side axis). Variable impact (right side axis) evidenced with blue line.

Supplementary Files

This is a list of supplementary files associated with this preprint. Click to download.

- supplementmaterial.docx